Changes in Soil Temperature and Active-Layer Thickness During the 20th Century in a Region in Western Canada

Wenjun Chen, Yu Zhang and Josef Cihlar
Canada Centre for Remote Sensing, Natural Resources Canada,
588 Booth Street,
Ottawa, ON, Canada, K1A 0Y7

Sharon L. Smith and Daniel W. Riseborough
Geological Survey of Canada,
601 Booth Street, Natural Resources Canada,
Ottawa, ON, Canada, K1A OE8

Submitted to ***Journal of Geophysical Research***

Corresponding author:

Yu Zhang
Environmental Monitoring Section
Canada Centre for Remote Sensing
Natural Resources Canada
588 Booth Street, 4th floor
Ottawa, ON, Canada
K1A 0Y7
Tel: 1-(613) 947-1367
Fax: 1-(613) 947 1383
E-mail: yu.zhang@ccrs.nrcan.gc.ca

Abstract. Increases in active-layer thickness and permafrost degradation induced by climate warming may have profound socio-economic and eco-environmental consequences. Using a process-based model of Northern Ecosystem Soil Temperature (NEST) and data from climate records, remote sensing vegetation parameters, and soil features, we simulated soil temperature and active-layer thickness (ALT) for a region in western Canada during the twentieth century. The results showed that the region-averaged annual mean soil temperatures at different depths responded to air temperature forcing consistently during the twentieth century, but with reduced magnitudes in both long-term trend and interannual variation. From the 1900s to 1986-1995, ALT increased 124 cm (or 79%) in the isolated and sporadic discontinuous permafrost zones, 59 cm (or 37%) in the extensive discontinuous permafrost zone, and 20 cm (or 21%) in the continuous permafrost zone based on the current permafrost distribution map. The simulated results also indicated the disappearance of 17% of the permafrost in the discontinuous permafrost zone from the 1900s to 1940s, and another 22% from the 1940s to 1986-1995. General agreements were found when comparing the simulated results with soil temperature records at climate stations, ALT at survey sites, and rates of permafrost degradation interpreted from aerial photographs. Owing to differences in spatial scales, spatial coverage, and time periods, many of the comparisons were not strict 1-to-1 comparisons and should instead be viewed as indirect supporting evidence.

Key words: Active-layer thickness; Soil temperature; Permafrost degradation; Climate change impacts; Simulation.

1. Introduction

Northern high-latitude ecosystems have developed a fragile equilibrium with the permafrost environment over thousands of years. Several studies [*e.g., Morison et al., 2000; Serreze et al., 2000; Anisimov et al., 2001; Goulden et al., 1998*] suggest that climate change since the industrial revolution may have disrupted this equilibrium. Increases in air temperature during the 20th century [*Zhang et al., 2000; Beltrami and Mareschal, 1991*] may have resulted in increases in active-layer thickness (ALT) and permafrost degradation, which in turn may damage building foundations and infrastructure [*Nelson et al., 2001*], impact on landscapes and ecosystems, and lead to the release of carbon stored in frozen soils. Key questions in permafrost-climate change studies are: How widespread has permafrost degradation been in the northern high latitudes during the 20th century? Will projected climate warming cause increased rates of permafrost degradation and the associated disruption to northern ecosystems and lifestyles of the local communities? Answers to these questions are required to estimate the implication of potential carbon release to the atmosphere and to better prepare northern communities to adapt to climate change.

Several studies have addressed these important issues using different approaches. *Smith and Burgess* [*1998*] assessed the sensitivity of permafrost to climate warming based on the buffer layer model of *Luthin and Guymon* [*1974*], which qualitatively links the atmospheric climate to subsurface climate considering the thermal properties of the ground. *Woo et al.* [*1992*] projected the shifts in the boundaries of continuous and discontinuous permafrost zones assuming surface temperature increases 4-5 ºC. *Anisimov and Nelson* [*1996*] estimated the distribution of permafrost in the Northern Hemisphere under an assumed 2 ºC global warming based on a frost index model. *Kettles et al.* [*1997*] assessed the changes in permafrost zones in Canada by comparing the current distribution of permafrost zones with the results projected by *Anisimov and Nelson* [*1996*]. *Anisimov et al.* [*1997*] simulated the changes in ALT in the Northern Hemisphere under climate change scenarios using a semi-empirical method. Based on this method and the distributions of soil texture and ground ice, they evaluated the risk of ground subsidence in the circum-Arctic permafrost region [*Nelson et al., 2001; 2002*]. *Henry and Smith*

[*2001*] produced a map of near-surface ground temperature in the permafrost regions of Canada based on a functional model of permafrost-climate system. *Malevsky-Malevich et al.* [*2001*] simulated the distribution of soil temperature and ALT in Russia based on solving a one-dimensional heat transfer equation assuming the monthly air temperature equals the mean surface temperature. These results are generally for equilibrium conditions (except *Malevsky-Malevich et al.* [*2001*]) and without explicitly considering the interactions among soil, vegetation, hydrology and climate. In addition, several researchers have been monitoring the changes in ALT and permafrost distribution based on in situ measurements and interpretation of aerial photographs (e.g., , *Brown et al., 2000; Thie, 1974; Vitt et al., 2000*). It is necessary however, to develop a process-based model based on these measurements so that we can assess the transient responses of permafrost conditions to climate change for different tempo-spatial scales, including the interactions among soil, vegetation and climate.

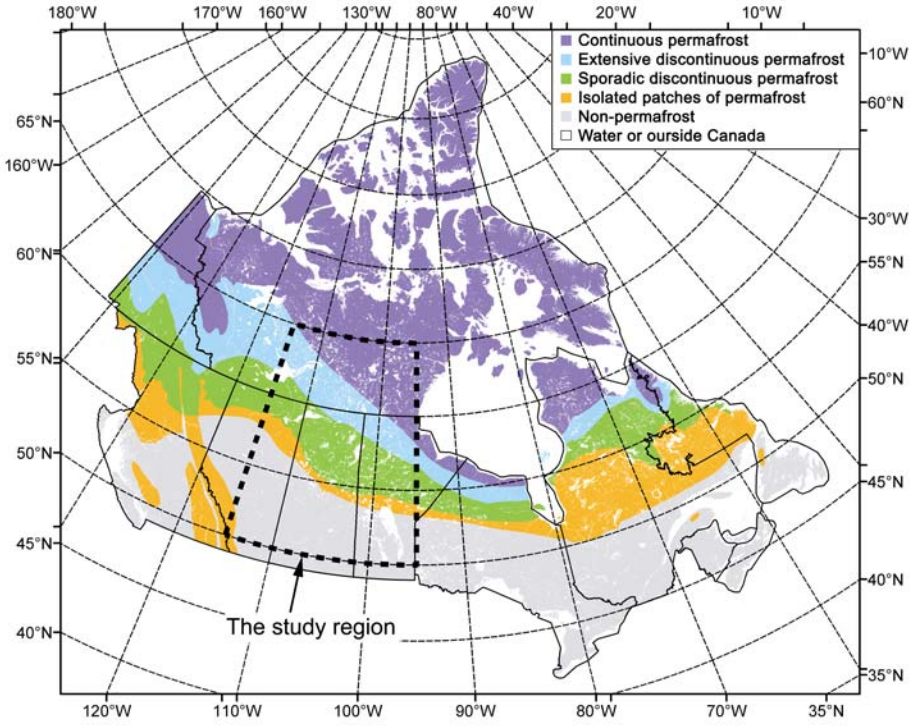

Figure 1. The study region (115-95 °W longitude and 50-65 °N latitude) and the distribution of permafrost types in Canada [*Heginbottom et al., 1995*].

In this study, a process-based model of Northern Ecosystem Soil Temperature (NEST) was developed. The model simulates soil temperature by solving the heat conduction equation, with the upper boundary conditions on the ground surface (or snow surface during winter) being determined based on energy balance and the lower boundary set at a depth of 35 m being defined by the geothermal flux. The effects of climate, vegetation, organic layers, soil texture, snowpack, and soil moisture on ground thermal dynamics are quantified based on energy and water transfer in soil-vegetation-atmosphere systems. Detailed description and validation analysis of the model are presented in a companion paper [*Zhang et al., 2003*]. In this paper, we report the results of application of the model to a region in western Canada for the climate effects on soil thermal regimes during the 20th century.

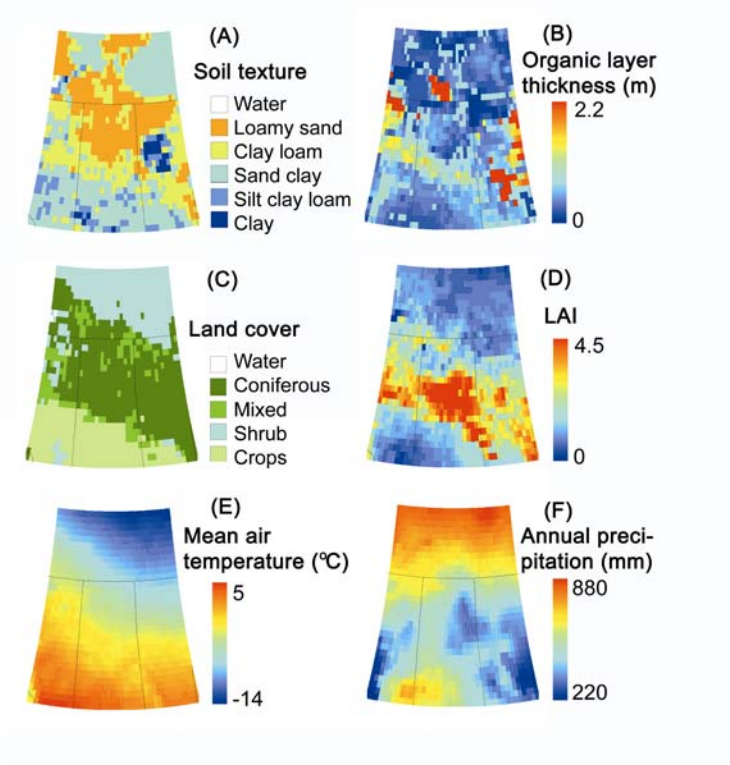

Figure 2. Spatial distributions of A) soil texture, B) organic material thickness, C) land cover types, D) summertime leaf area index, E) mean annual air temperature (1901-1995), and F) averaged annual precipitation (1901-1995).

The region is bounded from 115 °W to 95 °W longitude and from 50 °N to 65 °N latitude (Figure 1), including the Prairie Provinces, south-eastern Northwest Territories and south-western Nunavut in Canada. This region was selected because it provides a good representation of the ranges of climate, soil, vegetation and permafrost conditions, and climate change over the northern high latitudes; permafrost in this region might be very sensitive to climate change [*e.g., Smith and Burgess, 1998*]; and there are more studies and measurements of permafrost distribution and degradation in this region (*Zoltai, 1971; Thie, 1974; Nelson, 1986; Halsey et al., 1995; Vitt et al., 2000*). The mean annual air temperature in this region ranges from –14 °C to 5 °C, and annual precipitation varies from 215 mm to 820 mm based on climate data from 1901 to 1995. Surface organic layer ranges from 0 cm to > 2 m in thickness and it is underlain by different types of mineral soils. Vegetation types found in this region include deciduous, mixed forests, coniferous forests and tundra, with summertime leaf area index (LAI) varying from 0 to 4.5 (Figure 2). The region spans the four permafrost zones defined by *Heginbottom et al.* [*1995*] from isolated permafrost to the continuous permafrost zones (Figure 1. Because permafrost distribution and ALT change with climate conditions, the current boundaries of the permafrost zones are used as a spatial reference in this study). Annual mean air temperature increased by up to 4 °C during the 20th century in the center of this region, while southeastern areas experienced a cooling trend. Changes in soil temperature and ALT were simulated from 1901 to 1995 for this region at 0.5-degree latitude/longitude spatial resolution. Data sources and treatment are described in Section 2, followed by the simulation results in Section 3. Section 4 gives some comparisons with measurements and other estimates.

2. Data Sources and Treatment

2.1. Vegetation and soil data

Vegetation types were determined based on the 1 km spatial resolution land cover map of Canada derived from AVHRR [*Cihlar et al., 1999*]. LAI was derived from AVHRR 10-day composition images [*Chen J.M. et al., 2002*]. To match the spatial resolution of climate data, the 1 km resolution images were aggregated to 0.5-degree latitude/longitude

based on the dominant vegetation type in a grid cell for land cover, and based on the average for LAI. Water bodies are excluded in the calculation.

Soil texture, bulk density and organic content were extracted from the soil landscapes of Canada database [*Shields et al., 1991; Tarnocai and Lacelle, 1996*]. There are about 15000 polygons in the database covering Canadian landmass. Each polygon contains up to 10 components (with area percentage of composition), and each component includes 3 soil layers. The first layer is the surface organic layer for mineral soils or the layers above the permanent water table for peatlands. So we directly used this layer as the forest floor. If the organic content in deeper layers was higher than 17%, these layers were considered as peat layers, other wise they were considered as mineral layers. The thickness of the forest floor and the peat layers were calculated as the weighted averages of all the components in a polygon, excluding water bodies and rock. The organic carbon content in mineral soil layers was estimated as the weighted average of organic carbon content of the components in their mineral soil layers. The distribution of soil organic carbon in deeper soils (not available in the database) was assumed to decrease 50% for every 20 cm following *Jobbagy and Jackson* [*2000*]. The soil texture of a polygon was determined as the soil texture of the dominant component. We first interpolated these polygon data to 1 km spatial resolutions, and then aggregated them to 0.5-degree latitude/longitude grid cells based on the dominant type in a cell for soil texture, and based on the averages for forest floor thickness, bulk density and soil organic carbon content.

Excess ice content was set to 10% for both the continuous permafrost and extensive discontinuous permafrost, 5% for sporadic discontinuous permafrost, and 0% for other areas, based on the permafrost map of Canada [*Heginbottom et al., 1995*]. *Pollack et al.* [*1993*] reported a range of 0.02 to 0.056 $W \cdot m^{-2}$ for the geothermal heat flux in this region. Since there was no obvious spatial pattern in their reported data, an average value of 0.041 $W \cdot m^{-2}$ was used for the entire region.

2.2. Climate data

The gridded climate data set used in this study had a 0.5° latitude/longitude spatial resolution globally and a monthly temporal resolution from 1901 to 1995 [*New et al., 2000*]. It includes monthly means of air temperature, temperature diurnal range, water

vapor pressure, cloudiness, monthly total precipitation, and monthly total wet-days. This dataset was interpolated from station measurements considering topographic corrections.

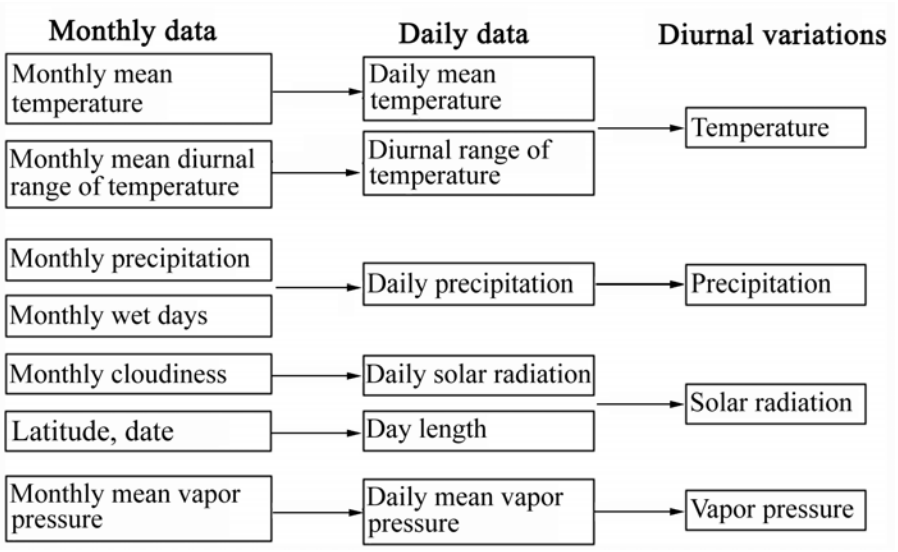

Figure 3. The scheme for scaling monthly climate data down to 30-minute intervals.

A short time step (e.g., 15-30 minutes) was used to ensure the stability of the calculation in the NEST model. Since the original climate data have a temporal resolution of a month, temporal down-scaling was required. First, daily values were estimated based on monthly data, and then, the diurnal changes were derived from the daily means (Figure 3). Daily mean temperature, diurnal temperature range, vapor pressure and cloudiness were linearly interpolated from their monthly means, and then modified for wet-days (precipitation > 0.1 mm) or dry-days. Generally, diurnal temperature range and daily mean air temperature are lower, and cloudiness and vapor pressure are higher on wet-days. The following equations were used to estimate the daily means of the above elements for wet-days and dry-days:

$$Y_{wet} = Y - \Delta Y \quad (1)$$

$$Y_{dry} = \frac{Y \cdot D_m - (Y - \Delta Y) D_{wet}}{D_m - D_{wet}} \quad (2)$$

where Y_{wet} and Y_{dry} are daily means of an element (i.e. temperature, temperature range, vapor pressure, and cloudiness) for a wet-day and a dry-day, respectively. Y is the daily mean linearly interpolated based on the monthly means (without considering wet-day and dry-day effects). D_m and D_{wet} are the total days in a month and the total wet-days in the month, respectively. ΔY is the difference of an element between the monthly mean (including wet and dry days) and the mean in wet-days. The average value of ΔY was determined from daily climate data (1975 to 1995) at climate stations in the study region. ΔY was 1.5 °C for diurnal temperature range, 1.1 °C for daily mean temperature, –0.1 for cloudiness, and –0.6 mb for vapor pressure.

Diurnal variation of air temperature was estimated following *William and Logan* [*1981*] with a sine function for daytime and an exponential function for nighttime. The day length (DL) was calculated based on latitude and Julian date [*Spitters et al., 1986*]. Daily solar radiation was estimated based on cloudiness following *Penman* [*1948*]:

$$R_d = R_0\left[a + b\left(1 - Cld\right)\right] \qquad (3)$$

where R_d is the daily solar radiation ($J \cdot m^{-2} \cdot d^{-1}$), *Cld* is the cloudiness (fraction), R_0 is the daily clear sky solar radiation estimated based on latitude and Julian date [*Spitters, et al., 1986*], a and b are parameters (a = 0.18, b = 0.55. *Penman, 1948*). Diurnal variation of solar radiation was estimated by a sine function [*Chung and Horton, 1987*]

$$R = 0.5\pi R_d / \left(3600 DL\right) \sin\left[\pi\left(t - 12 + 0.5DL\right)/DL\right] \qquad (4)$$

where R is the solar radiation ($W \cdot m^{-2}$) at time t. The diurnal change in vapor pressure was not considered, although vapor pressure deficit changes because air temperature changes diurnally. There were no wind speed data in this climate dataset [*New et al., 2000*]; an above-canopy mean wind speed of 3.0 $m \cdot s^{-1}$ was therefore used, based on the measurements at an aspen forest site in 1994 and 1996 [*Chen W. et al., 1999*].

A three-step approach was used to determine 30-minute precipitation distribution from the monthly total precipitation and wet days given in the dataset of *New et al.* [*2000*]. First, the distribution of wet-days within a month was determined as a random distribution. Second, the amount of precipitation on a wet-day was estimated based on the principle that light precipitation events occur more frequently than heavy ones, and this pattern can be described by an exponential distribution [*Richardson, 1981; Hann, 1977*]:

$$P_i = \frac{P'_i}{\sum_{i=1}^{n} P'_i} P_m \quad (5)$$

and

$$P'_i = -\ln(R_u)/A + x_0 \quad (6)$$

where P_i is amount of precipitation on a wet-day (mm), P_m and n are total amount of precipitation and number of wet-days in a month, respectively. R_u is a random number (ranging from 0 to 1), A and x_0 are parameters of the exponential distribution, equaling 0.3 and –3 mm, respectively, based on daily precipitation measurements at climate stations in the study region. Finally, the precipitation on a wet-day was treated as one precipitation event and distributed randomly within this day.

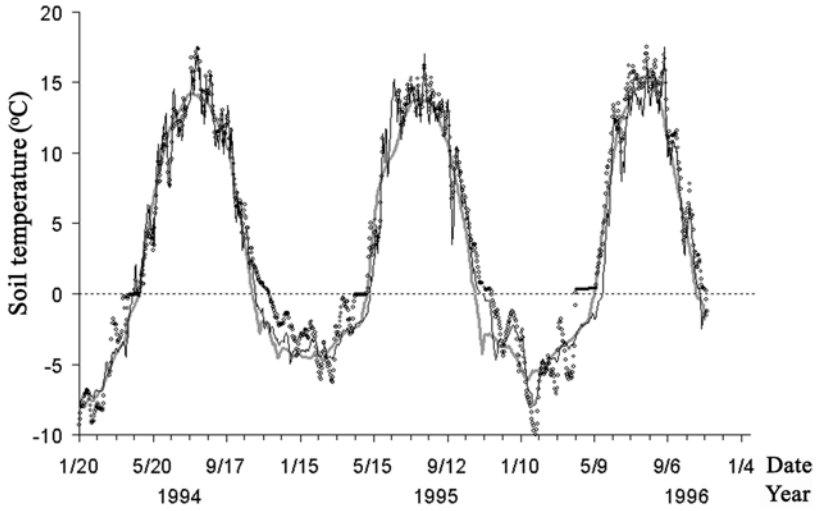

Figure 4. Comparison between the soil temperatures simulated using measured 15-minutes climate data as input (fine back curves) and using monthly climate data as input (grey curves). The measured daily soil temperatures (dots) were included as well.

Generally, changes in soil temperature represent the cumulative effects of current and previous climatic conditions, with the influence of earlier climatic conditions becoming more important in deeper soil layers due to a lag in the propagation of temperature changes. Consequently, the downscaling of monthly climate input data in a fashion as

described above may still produce reasonable soil temperatures, compared to those calculated using climate data of high temporal resolution such as 15 minutes. This hypothesis was tested for soil temperature estimation at an old jack pine site (53.92 °N, 104.69 °W) [*Baldocchi et al., 1997*]: one simulation used the measured 15-minute climate data as input, while the other used the monthly mean values as input (then downscaled to 15-minutes time scale). The results generally support this hypothesis (Figure 4).

2.3. Initialization

The initial climate conditions for a given month were obtained by first developing a linear relationship between a climate variable and the year from 1901 to 1995, and then using the relationship to extrapolate the variable for each month to the year 1900. The initial soil thermal and moisture conditions and snowpack were determined by iteratively running the model after setting preliminary estimates. The preliminary estimate for soil moisture was set to the field capacity of the soil type for the top 2 m layers, and saturation for the deeper layers. The preliminary estimate for snowpack was determined as the total precipitation when temperature was < 0 °C during July to December (simulation began on January 1) with an average snow density of 200 $kg \cdot m^{-3}$. The preliminary estimate of soil temperature was determined from a cosine function of Julian date with a delay in phase and exponential decrease in amplitude with depth. Using these input values, the model was then run iteratively until a stable soil temperature conditions were achieved (i.e., difference in annual mean soil temperature < 0.001 °C). The numerical exercise shows that the final stabilized initial conditions are not sensitive to the preliminary estimates of the snowpack, soil thermal and hydrological conditions, but a better preliminary estimate may need less iteration to achieve stability.

3. Results and Analysis

3.1. Soil temperature changes during the 20th century

Figure 5 shows the area-averaged annual mean soil temperatures at 0.2, 1, 10, and 35 m depth and the corresponding air temperature for the study region during the 20th century (from 1901 to 1995). During this period, the annual mean air temperature increased by 1.5 °C, while annual mean soil temperatures at 0.2, 1, 10, and 35 m depth

increased only 0.9, 0.9, 0.7, and 0.6 °C, respectively, based on a linear fit to the data. Figure 5 also shows reduced inter-annual variation for soil temperature in deeper layers compared to that of air temperature.

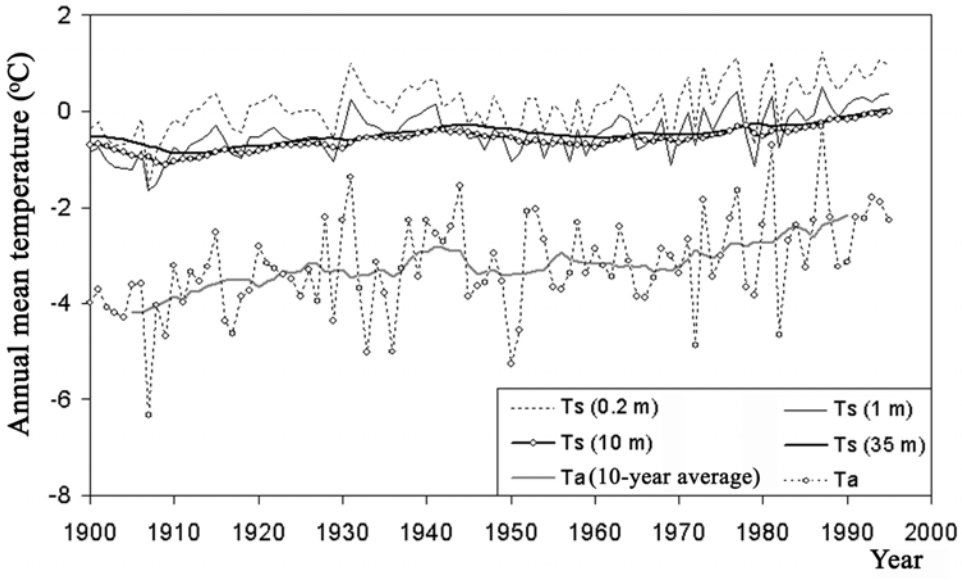

Figure 5. Variations of annual mean soil temperature (Ts) at different depths and annual mean air temperature (Ta). Values are averages of all the grid cells in the study region.

The temporal patterns of mean air temperature and mean soil temperature in the summer months are similar (Figure 6A). For the months of June, July and August, mean air temperature increased by 1.7 °C and soil temperature at the 0.2 m depth increased by 2.2 °C from 1901 to 1995. However, significant differences exist in the long-term trends and in interannual variation between mean air temperature and soil temperatures during the winter months (Figure 6B). For the months of January, February and March, mean air temperature increased by 3.3 °C, while mean soil temperature at the 0.2 m depth increased only by 1.1 °C from 1901 to 1995. Much of the decoupling between air temperature and soil temperature during the winter months may be explained by the insulation of snowpack and the changes in snowpack thickness (Figure 6C). The simulated snowpack thickness decreased by 6 cm from 1901 to 1995. A similar widespread decreasing trend in snowpack thickness between 1946 and 1995 (based on data from 122 Canadian climate stations) has been reported by *Brown and Braaten*

[*1998*]. A thinner snowpack favors heat loss from the ground during the winter months, and thus decreases soil temperature, and may offset the climate warming effects on soil temperature in wintertime. The effect of snowpack thickness on soil temperature has been reported by other studies as well [*e.g., Pavlov, 1994; Goodrich, 1982*].

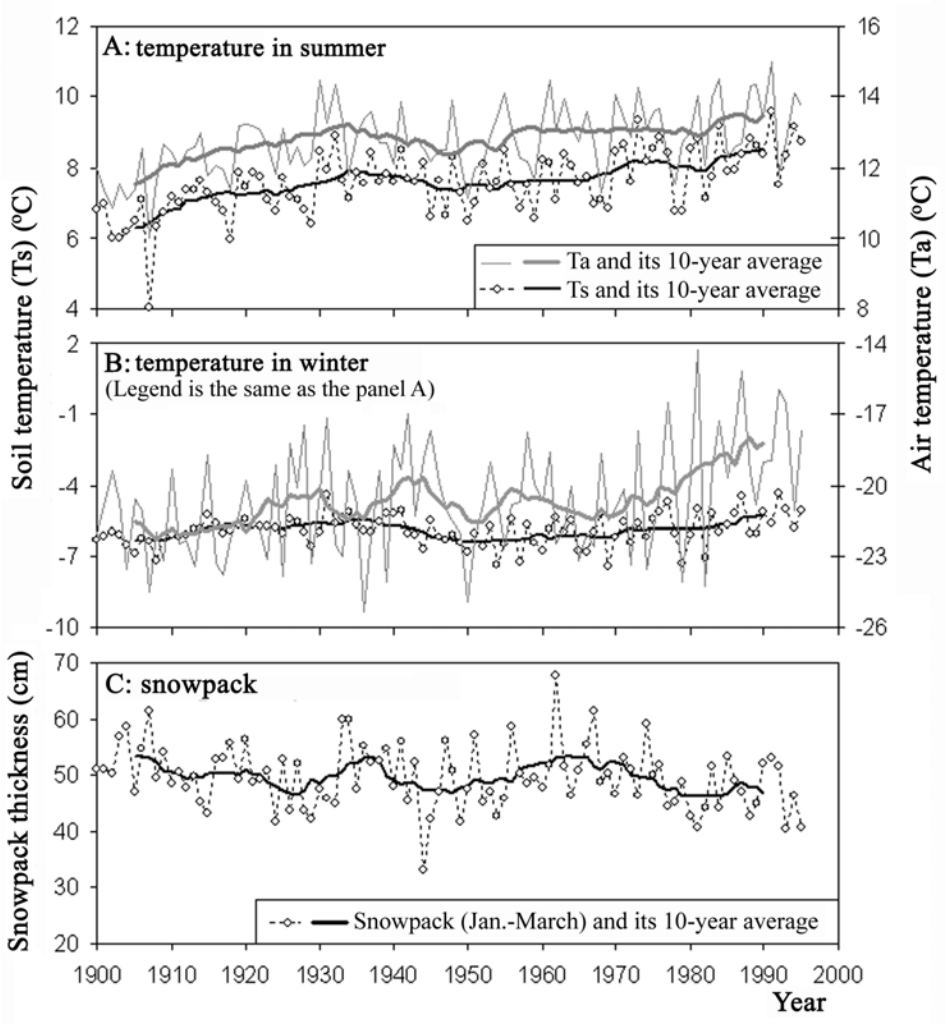

Figure 6. The temporal variations of soil temperatures (Ts) at 20 cm depth in summertime (June, July and August) and in wintertime (January, February, and March), comparing with the changes in air temperatures (Ta) and snowpack thickness. Values are averages of all the grid cells in the study region.

Measurements show that atmospheric climate warming during the 20th century has resulted in increases in ground temperature at depths greater than 35 m [*Lachenbruch and Marshall, 1986*], so that our assumed constant geothermal flux at this depth might

produce some artifacts about the long-term trend of soil temperature and ALT. To test this effect, we run the model for a permafrost site (59.75 ºN, 100.25 ºW) using the geothermal flux of 0.01 $W \cdot m^{-2}$ and 0.10 $W \cdot m^{-2}$, and using the lower boundary at a depth of 75 m, and comparing with the baseline results (Lower boundary is at 35 m depth, and the geothermal flux is 0.041 $W \cdot m^{-2}$). The results show that the soil temperatures at shallow depths are almost identical (difference is less than 0.05 ºC) among these cases, and differences in ALT among them are less then 0.05 cm (results are not show because these differences are too small compared to their fluctuations from year to year). There are some differences for soil temperature at deeper layers among these cases, but their temporal trends are similar after reaching equilibrium conditions in 1990 (Figure 7). These tests show that our assumed constant geothermal flux at 35 m depth have very little effects on soil thermal conditions and their temporal trend at shallow depths.

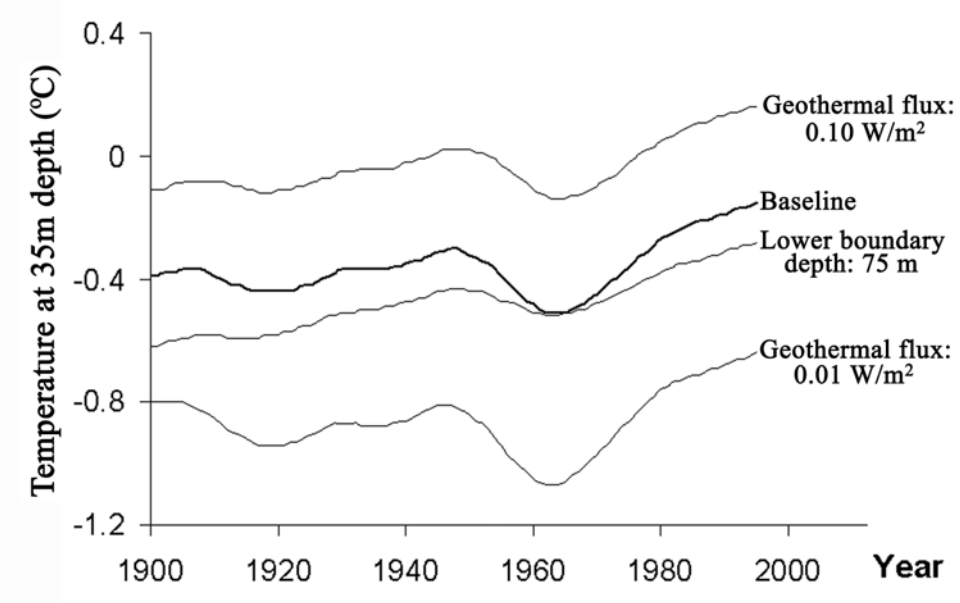

Figure 7. Comparison of the simulated ground temperature at 35 m depth using different geothermal flux and lower boundary depths for a permafrost site (59.75 ºN, 100.25 ºW).

In addition to the differences in long-term trend and the annual amplitude between air temperature and soil temperature, they differed also in absolute values. For example, the annual mean soil temperature at the 0.2 m depth averaged from 1901 to 1995 was 3.4 °C

higher than that of air temperature (Figure 5). *Brown* [*1970*] reported a similar difference of 3 °C between annual mean air and soil temperatures for Canada's permafrost areas. As shown in Figure 6, the difference in annual mean air and soil temperatures was mainly due to the much higher soil temperature during the winter months because of the insulating effect of the snow cover.

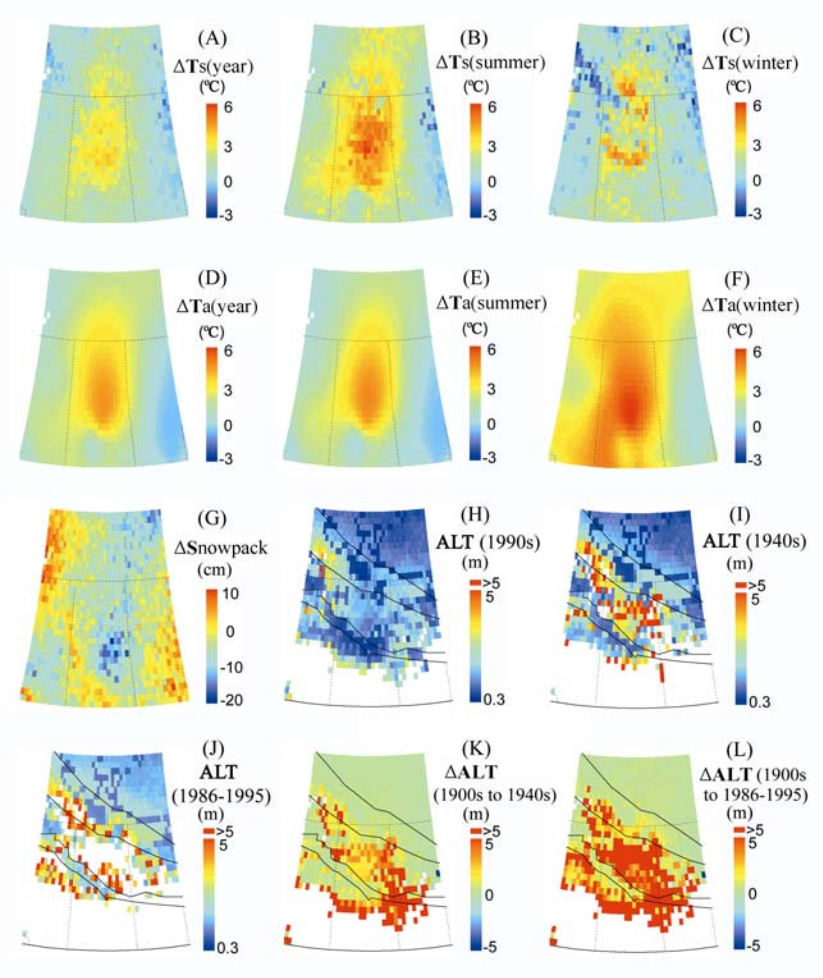

Figure 8. Spatial distributions of the changes in soil temperature (A, B, and C), air temperature (D, E, and F), snowpack thickness during the winter (G), and ALT (K and L). The decadal means of ALT in the 1900s (H), the 1940s (I) and 1986-1995 (J) are also shown. In plates H to L, white area represents the cells without permafrost. The lines in plate H to L are the southern boundaries of permafrost zones delineated by *Heginbottom et al.* [*1995*] (from the top to bottom, they are for the southern limits of continuous, extensive discontinuous, sporadic discontinuous, and isolated permafrost zones, respectively).

The temporal changes in soil temperature during the 20th century were not spatially uniform. As shown in Figure 8, annual mean soil temperature at the 0.2 m depth in northern Saskatchewan increased more rapidly, by 3 °C from 1901 to 1995, but decreased in southwest Manitoba. A similar spatial pattern was found for the changes in summer mean soil temperature. In the winter, the increase in air temperature was more significant (up to 6 °C) and widespread from 1901 to 1995, but the soil temperature increase during these months occurred in a much smaller area and distributed heterogeneously. This may be explained by both temporal and spatial variations in snowpack thickness. Generally, snowpack thickness decreased in areas where winter mean air temperature increased, and vice versa. The combination of changes in winter mean air temperature and in snowpack thickness thus resulted in smaller and more heterogeneous changes in winter mean soil temperature.

3.2. Changes in active-layer thickness during the 20th century

Figure 8 also shows the simulated ALT for areas underlain by permafrost for the periods of the 1900s, 1940s, and 1986-1995. ALT varied from 35 cm to more than 500 cm. ALT of > 500 cm mainly occurred in the discontinuous permafrost zone, as defined by *Heginbottom et al.* [*1995*]. For the period between the 1900s and the 1940s during which air temperature increased steadily, ALT increased significantly in the middle and southern portion of permafrost region in the study region. In some areas, permafrost disappeared completely over this period. An even higher rate of air temperature increase since the 1970s resulted in further widespread disappearance of permafrost in the middle and southern portion of the study region. On average, ALT increased by 79%, 37% and 21% from 1901 to 1995 for the isolated and sporadic discontinuous permafrost zones (considered as one zone here), the extensive discontinuous permafrost zone, and the continuous permafrost zone, respectively, based on the current permafrost zone boundaries from *Heginbottom et al.* [*1995*] (Figure 9A). Large increases in ALT occurred in areas where soil temperatures were within a few degrees of 0 °C, where permafrost was more sensitive to climate warming [*Smith and Burgess, 1998*].

Figure 9B also shows the number of the grid cells in different permafrost zones of the permafrost map [*Heginbottom et al., 1995*] in the 1900s, 1940s, and 1986-1995. In the isolated and sporadic discontinuous permafrost zones, the area underlain by permafrost

was reduced by 24% between the 1900s and the 1940s, and further reduced by 33% by the decade of 1986-1995. The decrease in the area underlain by permafrost was much less in the extensive discontinuous permafrost zone: 4% by the 1940s and 5% by the decade of 1986-1995. There was no permafrost disappearance for the continuous permafrost zone.

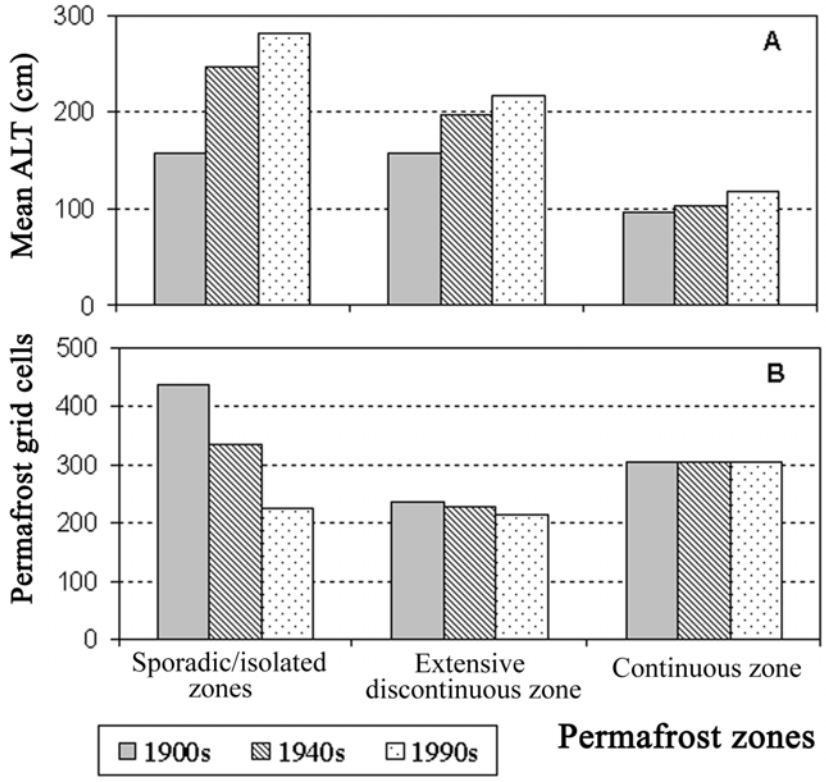

Figure 9. Mean active-layer thickness and the number of permafrost grid cells in the 1900s, 1940s and 1986-1995 for the current permafrost zones delineated by *Heginbottom et al.* [*1995*]

4. Comparison with Measurements and Other Estimates

4.1. Soil temperature

There are several climate stations in the study region that have long-term records of soil temperature, and can be used to compare with the simulated results. However, strict one-to-one comparisons cannot be made using these soil temperature data because they are point measurements and the site conditions of the climate stations can differ

significantly from their surrounding areas that are represented in the 0.5-degree latitude/longitude grid cells. For example, the magnitude of soil temperature response to climate change at a site under dense vegetation with a thick surface organic layer could be much smaller than that at a site where the ground is covered by short grass without much surface organic layer. The differences in vegetation and surface organic layers may also alter the snow accumulation in the winter and thus the winter soil temperature.

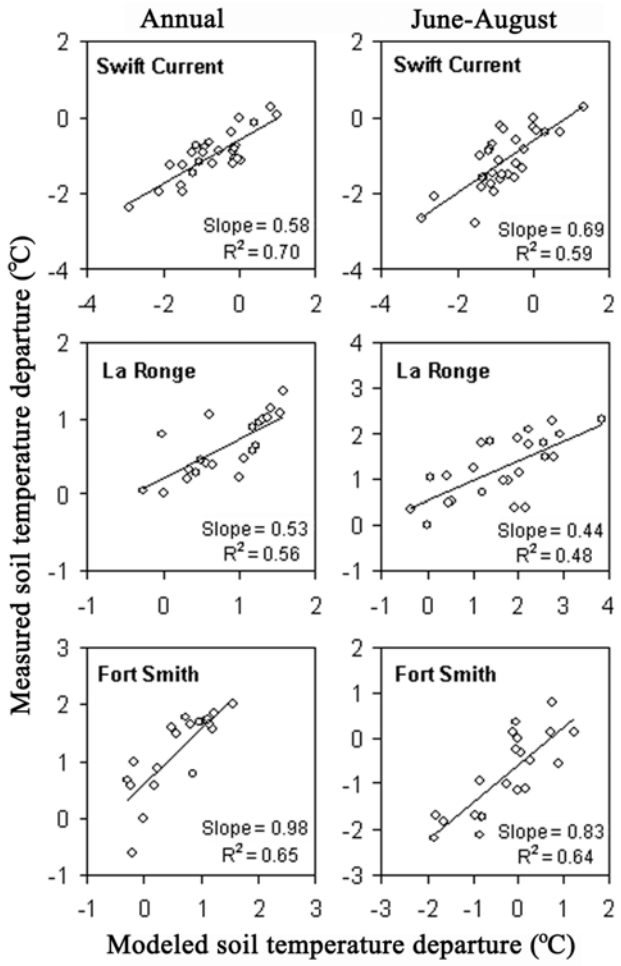

Figure 10. Comparisons between simulated and observed changes in annual mean soil temperature expressed as departures from the earliest record for each site. The measurements were from climate stations along a latitude gradient: Swift Current (50.27 ^{o}N, 108.73 ^{o}W), La Ronge (55.13 ^{o}N, 105.27 ^{o}W), and Fort Smith (60.03 ^{o}N, 111.93 ^{o}W).

Figure 10 shows comparisons of measured and simulated soil temperature departures from the first measurement record year at 20 cm depth for three representative climate stations from Environment Canada: Swift Current, La Ronge, and Fort Smith. The Swift

Current station is located in a grass and shrub land with LAI of 0.4 and a surface organic layer of 6 cm. As expected, the changes in soil temperature at this climate station, in reference to the temperature in 1964, were consistent with but larger than that of the surrounding grid cell, for both annual mean soil temperature and June-August mean soil temperature. The magnitude of the response was further reduced in the area surrounding the La Ronge climate station, which was a mature coniferous forest area with a LAI of 3.4 and a surface organic layer of 30 cm. For the Fort Smith station, which was surrounded by low vegetation with LAI of 0.4 and a surface organic layer of 6 cm, we found similar responses in both the pattern and magnitude between the climate station and its surrounding area.

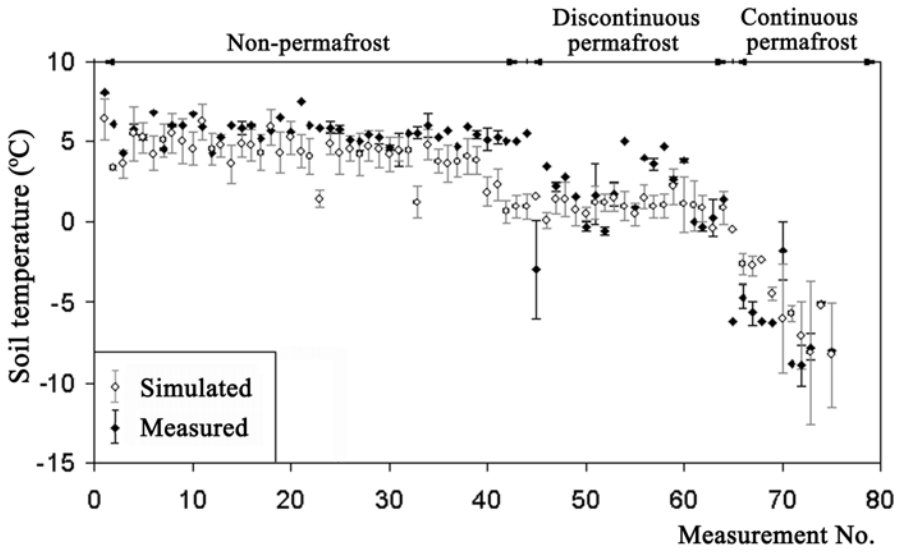

Figure 11. Comparison between simulated and measured near-surface soil temperature for different permafrost zones and latitude (sites were arranged with increasing latitude within each permafrost zone). The measurements were extracted from the soil temperature database [*Smith and Burgess, 2000*]. The measurements were aggregated into a mean and a range if more than one measurement was available in a grid cell. Measurements were conducted at different depths and time periods. A period of 1950-1980 was used if no measurement period was indicated in the database.

A more direct comparison may be possible in terms of soil temperature spatial distribution using soil temperature measurements at natural sites complied by *Smith and Burgess* [*2000*]. Some sites only had one record at a depth of 10-15 m where seasonal temperature fluctuations were minimum, while for other sites annual mean temperatures

at shallower depths were available. There are 73 grid cells where 1 to 5 measurements are available (Figure 11). The error bars show the range in observed values resulting from differences in site location and conditions and period of measurement. The error bars of the simulated results are the ranges of annual mean soil temperatures corresponding to the years when measurements were available. The simulated results showed similar trends and were in general agreement within the ranges of measurements.

The simulated temperatures were consistently lower than observed temperatures by about 5 °C at site number 23, 33, and 41-45. These sites were covered by dense coniferous forests with higher LAI, and located near the southern limit of the permafrost zone. Mean summer soil temperatures change abruptly between adjacent cells in this region. This may be due to the treatment of summertime LAI as a constant value over the whole simulation period. Disturbances such as forest fire would cause substantial change in LAI, and fire return frequency was quite high in this region [*Amiro, 2000*]. Therefore, it should be a future priority to incorporate NEST with vegetation dynamics, such as linking with the Integrated Terrestrial Ecosystem Carbon-budget model (InTEC) [*Chen W. et al., 2002; 2000a, b; Chen J.M. et al., 2000*].

4.2. Active-layer thickness

There are 12 records of ALT measurements in the national permafrost database of *Smith and Burgess* [*2000*] (Figure 12). The observed ALT in the discontinuous permafrost zone varied from < 50 cm to greater than 400 cm. In the continuous permafrost zone, ALT is generally less than 300 cm. The simulated results showed a similar pattern and were generally within this range of the measurements. The measurements usually indicated a wide range of ALT, probably due to the effects of local site conditions, whereas the simulated results represent the mean conditions at a 0.5-degree latitude/longitude spatial scale and thus tend to be in the middle of the measured range.

There are no long-term active-layer monitoring sites in our study region. *Brown et al.* [*2000*] analyzed the measurements of ALT around the world (mainly conducted in the 1990s in continuous permafrost areas), and indicated that ALT responds consistently to the forcing of climate, especially temperatures in summer, although the records are not long enough to indicate a long-term trend. The simulated changes of ALT also show its

responses to climate warming, although it is difficult to compare directly because of the differences in scale and time of the observations.

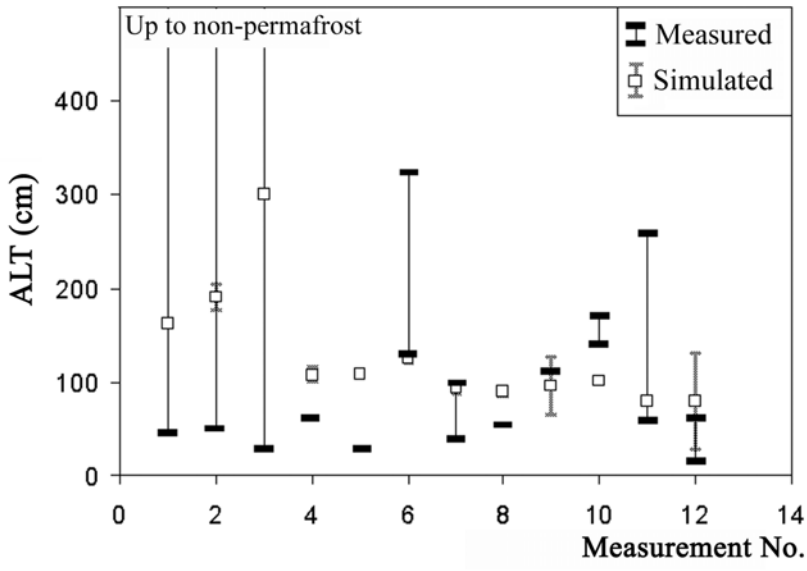

Figure 12. Comparison between simulated and observed active-layer thickness (ALT): point 1 was in the isolated permafrost zone, points 2 and 3 were in the discontinuous permafrost zone, and points 4-13 were in the continuous permafrost zone (ordered by increasing latitude). The measurements were extracted from the national permafrost database [*Smith and Burgess, 2000*].

4.3. Permafrost distribution and degradation

The simulated southern limit of permafrost (SLP) after the 1940s was very close to that of the current permafrost map, which was delineated mainly based on climate and field measurements from the 1950s to the 1980s [*Heginbottom et al., 1995*], but simulated SLP for the 1900s was up to 200 km south of that on the current permafrost map. Several studies suggested that permafrost existed further south in the early 20th century than at present [*Zoltai, 1971; Thie, 1974; Vitt et al.; 2000*]. *Halsey et al.* [*1995*] and *Vitt et al.* [*2000*] mapped the degradation of permafrost in peatlands through interpreting internal lawn distribution using aerial photographs, because the degradation of permafrost in peatlands generally forms internal lawns with unique vegetation features. They delineated SLP for the end of Little Ice Age (about 1850), which was up to 200 km south of SLP delineated in the permafrost map of Canada [*Heginbottom et al., 1995*]

(Figure 13). Continuous warming of climate may be the major reason for this difference in SLP, and this change was similar to the simulated SLP change (Figure 8), although the local details were different because of the differences in data sources and spatial scale, and the influence of local soil and hydrological conditions [*Nelson, 1986*].

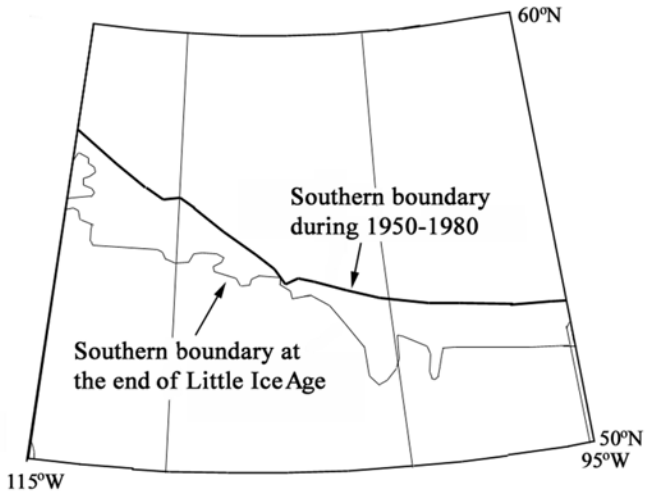

Figure 13. The northward retreat of the southern boundary of permafrost from the end of the Little Ice Age around 1850 [*Vitt et al.*, 2000] to 1950-1980 [*Heginbottom et al.*, 1995].

Thie [*1974*] studied the distribution of permafrost and its change in an area of 225 km^2 in central Manitoba (Latitude 54 ºN to the north shore of Lake Winnipeg, Longitude 99-98 ºW) based on aerial photographs taken from 1926 to 1946. He found that the percentage of land underlain by permafrost decreased from 60% to 15% from about 1850 to 1967 for this area. Our simulated results also showed disappearance of permafrost and significant increases in ALT in this area from the 1900s to 1940s (Figure 8). *Halsey et al.* [*1995*] and *Vitt et al.* [*2000*] estimated that 9% of permafrost disappeared in permafrost peatland area in the three Prairies Provinces of Alberta, Saskatchewan, and Manitoba

from the end of the Little Ice Age (around 1850) to 1949-1952 during which the aerial photographs were taken. For the period from 1950 to 1995 during which the studies of *Halsey et al.* [*1995*] and *Vitt et al.* [*2000*] did not cover, the study of *Jorgenson et al.* [*2001*] in central Alaska may serve as a good alternative reference. *Jorgenson et al.* [*2001*] estimated that permafrost in this area reduced by about 30% from 1949 to 1995.

The simulated results (Figure 9) indicated that within the present discontinuous permafrost zones, approximately 17% of the permafrost disappeared between the 1900s and 1940s and a further loss of about 22% from the 1940s to 1985-95. The modeled results were comparable to those of *Halsey et al.* [*1995*], *Vitt et al.* [*2000*] and *Jorgenson et al.* [*2001*]. The difference between these studies and the modeled results was largely due to the higher spatial resolution provided by the aerial photograph interpretation comparing to the spatial resolution used in the modeling. In addition, these studies were only for permafrost peatlands, while the present study included all ecosystem types.

5. Concluding Remarks

Using a process-based model of Northern Ecosystem Soil Temperature, and input data of historical climate, land cover and LAI from remote sensing, and soil features, the responses of the ground thermal regime and ALT of a large region in western Canada to climate change during the 20th century were investigated. Based on the analysis of the simulated results, the following conclusions can be drawn:

(1) From 1901 to1995, the region-averaged mean annual soil temperatures at 0.2, 1, 10, and 35 m depth increased only 0.9, 0.9, 0.7, and 0.6 °C, respectively, in response to the mean annual air temperature increase of 1.5 °C over the entire period, although substantial spatial variation existed. The reduced rate of increase in soil temperature could largely be explained by decreases in snowpack thickness associated with warming.

(2) Simulated ALT was generally in agreement with observed values. Averaged over the study region, the simulation showed that the mean ALT increased by 124 cm in the isolated and sporadic discontinuous permafrost zones, 58 cm in the extensive discontinuous permafrost zone, and 21 cm in the continuous permafrost zone from the 1900s to 1986-1995.

(3) The results of this study show that the area underlain by permafrost within the

present discontinuous zones decreased by 17% from the 1900s to the 1940s, and further reduced by 22% from the 1940s to 1986-1995. A northward shift in the southern limit of permafrost of about 200 km over the 20th century was simulated. These results are comparable with the estimates from aerial photographs.

Several research priorities must be addressed in order to further improve the simulation results, including increasing in the spatial resolution so that the simulation results are more comparable with site measurements, expanding the simulation to regions where long term active layer monitoring records are available so that strict testing may be carried out, and coupling with vegetation dynamics and biogeochemical models. In our previous studies on the long-term national carbon cycle [*Chen W. et al., 2000a, b; Chen J.M. et al., 2000*], we assumed that soil temperatures follow the long-term trend of annual mean air temperature but with the inter-annual amplitude reduced by 30%. This study indicated that the previous assumption oversimplified the situation and could introduce significant error in soil respiration estimation, especially at high latitudes where the winter is long and may contribute up to 20-30% of the annual total respiration [*Goulden et al., 1998; Chen W. et al., 1999*]. Coupling with the Integrated Terrestrial Ecosystem Carbon-budget model (InTEC) [*Chen W. et al., 2002; 2000a, b; Chen J.M. et al., 2000*] with NEST would improve the quantification of the carbon cycle, and may also improve the estimation of soil temperature and ALT themselves with the dynamics of vegetation and soil carbon dynamics, especially the effects of disturbances (e.g., fire, insects damage, and harvesting) on vegetation and forest floor.

Acknowledgement. The authors are grateful to Charles Tarnocai for providing the soil landscapes of Canada database and giving directions for using it. Thanks are also given to Joost Van der Sanden for reviewing the manuscript. The comments of three anonymous reviewers were very helpful in improving this manuscript. This study is supported by the Panel for Energy Research and Development (PERD), Canada's Climate Change Action Fund (CCAF), and the Long-term Space Plan (LTSP).

References

Amiro, B.D., J.B. Todd, B.M. Wotton, K.A. Logan, M.D. Flannigan, B.J. Stocks, J.A. Mason, D.L. Martell, and K.G. Hirsch, Direct carbon emissions from Canadian forest fires, 1959–1999, *Can. J. For. Res., 31,* 512–525, 2001.

Anisimov, O.A., B. Fitzharris, J.O. Hagan, R. Jeffries, H. Marchant, F.E. Nelson, T. Prowse, and D.G. Vaughan, Polar regions (Arctic and Antarctic), in *Climate Change: Impacts, Adaptation, and Vulnerability, The Contribution of Working Group II of the Intergovernmental Panel on Climate Change*, Third Assessment Review, 801-841 pp., Cambridge, U.K., Cambridge University Press, 2001.

Anisimov, O.A., N.I. Shiklomanov, and F.E. Nelson, Global warming and active-layer thickness: results from transient general circulation models, *Global and Planetary Change, 15,* 61-77, 1997.

Anisimov, O.A., and F.E. Nelson, Permafrost distribution in the Northern Hemisphere under scenarios of climatic change, *Global and Planetary Change, 14,* 59-72, 1996.

Baldocchi, D.D., C.A. Vogel, and B. Hall, Seasonal variation of energy and water vapor exchange rates above and below a boreal jack pine forest canopy, *J. Geophys. Res., 102,* 28939-28951, 1997.

Beltrami, H., and J.C. Mareschal, Recent warming in eastern Canada inferred from geothermal measurements, *Geophys. Res. Lett., 18,* 605-608, 1991.

Brown, R.D., and R.O. Braaten, Spatial and temporal variability of Canadian monthly snow depths, 1946-1995, *Atmosphere-Ocean, 36,* 37-54, 1998.

Brown, J., K.M. Hinkel, and F.E. Nelson, The circumpolar active layer monitoring (CALM) program: research designs and initial results, *Polar geography, 24,* 166-252, 2000.

Brown, R.J.E., *Permafrost in Canada: Its Influence on Northern Development,* 234 pp., University of Toronto Press, Toronto, Canada, 1970.

Chen, J.M., G. Pavolic, L. Brown, J. Cihlar, S.G. Leblanc, P.H. White, R.G. Hall, D. Peddle, D.J. King, J.A. Trofymow, E. Swift, J. van der Sanden, and P. Pellikka, Validation of Canada-wide leaf area index maps using ground measurements and

high and moderate resolution satellite imagery, *Remote Sensing of Environment, 80,* 165-184, 2002.

Chen, J.M., W. Chen, J. Liu, J. Cihlar, and S. Gray, Annual carbon balance of Canada's forest during 1895-1996, *Global Biogeochem. Cycles, 14*, 839-850, 2000.

Chen, W., T.A. Black, P.C. Yang, A.G. Barr, H.H. Neumann, Z. Nesic, M.D. Novak, J. Eley, R. Cuenca, Effects of climate variability on the annual carbon sequestration by a boreal aspen forest, *Global Change Biology*, 5, 41-53, 1999.

Chen, W., J.M. Chen, D.T. Price, and J. Cihlar, Effects of stand age on net primary productivity of boreal black spruce forests in Ontario, Canada, *Can. J. For. Res., 32,* 833-842, 2002.

Chen, W., J.M. Chen, and J. Cihlar, An integrated terrestrial carbon-budget model based on changes in disturbance, climate, and atmospheric chemistry, *Ecol. Model., 135,* 55-79, 2000a.

Chen, W., J.M. Chen, J. Liu, and J. Cihlar, Approaches for reducing uncertainties in regional forest carbon balance, *Global Biogeochem. Cycles, 14,* 827-838, 2000b.

Chen, W., T.A. Black, P.C. Yang, A.G. Barr, H.H. Neumann, Z. Nesic, P.D. Blanken, M.D. Novak, J. Eley, R.J. Ketler, and R. Cuenca, Effects of climatic variability on the annual carbon sequestration by a boreal aspen forest, *Global Change Biology, 5,* 41-53, 1999.

Chung, S., and R. Horton, Soil heat and water flow with partial surface mulch, *Water Resources Research, 23,* 2175-2186, 1987.

Cihlar, J., J. Beaubien, R. Latifovic, and G. Simard, *Land Cover of Canada 1995*, Version 1.1. Digital dataset documentation, Natural Resources Canada, Ottawa, Canada, 1999.

Goodrich, L.E., The influence of snow cover on the ground thermal regime, *Can. Geotech. J., 19,* 421-432, 1982.

Goulden, M.L., S.C. Wofsy, J.W. Harden, S.E. Trumbore, P.M. Crill, S.T. Gower, T. Fries, B.S. Daube, Fan S-M, D.J. Sutton, A. Bazzaz, and J.W. Munger, Sensitivity of boreal forest carbon balance to soil thaw, *Science, 279,* 214-217, 1998.

Halsey, L.A., D. Vitt, and S.C. Zoltai, Disequilibrium response of permafrost in boreal continental western Canada to climate change, *Climatic Change, 30,* 57-73, 1995.

Hann, C.T., *Statistical Methods in Hydrology,* 378 pp., The Iowa State University Press, Ames, Iowa, 1977.

Heginbottom, J.A., M.A. Dubreuil, and P.A. Harker, Canada-Permafrost, in *National Atlas of Canada* 5th edition, Natural Resources Canada, Ottawa, Canada, 1995.

Henry, K., and M. Smith, A model-based map of ground temperatures for permafrost regions of Canada, *Permafrost and Periglacial Processes, 12,* 389-398, 2001.

Lachenbruch, A.H., and B.V. Marshall, Changing climate: geothermal evidence from permafrost in the Alaskan Arctic, *Science, 234,* 689-696, 1986.

Luthin, J.N., and G.L. Guymon, Soil moisture-vegetation-temperature relationships in central Alaska, *J. of Hydrology, 23,* 233-246, 1974.

Jobbagy, E.G., and R.B. Jackson, The vertical distribution of soil organic carbon and its relation to climate and vegetation, *Ecological Applications,* 10, 423-436, 2000.

Jorgenson, M.T., C.H. Racine, J.C. Walters, and T.E. Osterkamp, Permafrost degradation and ecological changes associated with a warming climate in central Alaska, *Climatic Change, 48,* 551-579, 2001.

Kettle, I.M., C. Tarnocai, and S.D. Bauke, Predicted permafrost distribution in Canada under a climate warming scenario, *Current Research, Geological Survey of Canada, 1997-E,* 109-115, 1997.

Malevsky-Malevich, S.P., E.K. Molkentin, E.D. Nadyozhina, and O.B. Shklyarevich, Numerical simulation of permafrost parameters distribution in Russia, *Cold Regions Science and Technology, 32,* 1-11, 2001.

Morison, J., K. Agaard, and M. Steele, Recent environmental changes in the arctic: A review, *Arctic, 52,* 359-371, 2000.

Nelson, F.E., Permafrost distribution in central Canada: applications of a climate-based predictive model, *Annals of the Association of American Geographers, 76,* 550-669, 1986.

Nelson, F.E., O.A. Anisimov, and N.I. Shiklomanov, Climate change and hazard zonation in the circum-Arctic permafrost regions, *Natural Hazards, 26,* 203-225, 2002.

Nelson, F.E., O.A. Anisimov and N.I. Shiklomanov, Subsidence risk from thawing permafrost, *Nature, 410,* 889-890, 2001.

New M.G., M. Hulme, and P.D. Jones, Representing twentieth century space-time climate variability, Part II: Development of a 1901-1996 monthly terrestrial climate fields, *J. Climate, 13,* 2217-2238, 2000.

Penman, H.L., Natural evaporation from open water, bare soil and grass, *Proc. of Royal Society of London, A193,* 120-146, 1948.

Pavlov, A.V., Current changes of climate and permafrost in Arctic and sub-Arctic of Russia, *Permafrost and Periglacial processes, 5,* 101-110, 1994.

Pollack, H.N., S.J. Hurter, and J.R. Johnson, Heat flow from the earth's interior: analysis of the global data set, *Reviews of Geophysics, 31,* 267-280, 1993.

Richardson, C.W., Stochastic simulation of daily precipitation, temperature, and solar radiation, *Water Resources Research, 17,* 182-190, 1981.

Serreze, M.C., J.E. Walsh, F.S. Chapin III, T. Osterkamp, M. Dyurgerov, V. Romanovsky, W.C. Oechel, J. Morison, T. Zhang, and R.C. Barry, Observational evidence of recent change in the northern high-latitude environment, *Climatic Change, 46,* 159-207, 2000.

Shields, J.A., C. Tarnocai, K.W.G. Valentine, and K.B. MacDonald, *Soil Landscapes of Canada - Procedures Manual and User's Handbook,* 74 pp., Land Resource Research Centre, Research Branch, Agriculture Canada, Ottawa, Canada, 1991.

Smith, S.L., and M.M. Burgess, *Ground Temperature Database for Northern Canada,* Open File Report #3954, 57 pp., Geological Survey of Canada, Ottawa, Canada, 2000.

Smith, S.L., and M.M. Burgess, Mapping the sensitivity of Canadian permafrost to climate warming, *Current Research, Geological Survey of Canada, 1998-E,* 163-191, 1998.

Spitters, C.J.T., H.A.J.M. Toussaint, J. Goudriaan, Separating the diffuse and direct component of global radiation and its implication for modelling canopy photosynthesis. Part I: components of incoming radiation, *Agric. For. Meteorol., 38,* 217-229, 1986.

Tarnocai, C., and B. Lacelle, *Soil Organic Carbon Digital Database of Canada*, Eastern Cereal and Oilseed Research Centre, Research Branch, Agriculture and Agri-Food Canada, Ottawa, Canada, 1996.

Thie, J., Distribution and thawing of permafrost in the southern part of the discontinuous permafrost zone in Manitoba, *Arctic, 27,* 189-200, 1974.

Vitt, D.H., L.A. Halsey, and S.C. Zoltai, The changing landscape of Canada's western boreal forest: the current dynamics of permafrost, *Can. J. For. Res., 30,* 283-287, 2000.

William, J.P., and J.A. Logan, A model for diurnal variation in soil and air temperature, *Agricultural Meteorology, 23,* 205-216, 1981.

Woo, M., A.G. Lewkowicz, and W.R. Rouse, Response of the Canadian permafrost environment to climatic change, *Physical geography, 13,* 287-317, 1992.

Zhang, X., L.A. Vincent, W.D. Hogg, and A. Niitsoo, Temperature and precipitation trends in Canada during the 20th century, *Atmosphere-Ocean, 38,* 395-429, 2000.

Zhang, Y., W. Chen, and J. Cihlar, A Process-based model for quantifying the impact of climate change on permafrost thermal regimes, *J. Geophys. Res.*, 2003. (submitted).

Zoltai, S.C., Southern limit of permafrost features in peat landforms, Manitoba and Saskatchewan, *Geological Association of Canada Special Paper, 9,* 305-310, 1971.